REFLECTION OF SOUND FROM A LAYERED OCEAN BOTTOM

by

Homer P. Bucker and Halcyon E. Morris
US Naval Undersea Center
San Diego, California 92132
U.S.A.

(No Abstract received)

I. INTRODUCTION

This paper reviews the theory of how a horizontally stratified ocean bottom interacts with acoustic energy to effect sonar systems. At frequencies associated with active sonars ($\sim$ 2.5 to 15 kHz) the theory is well in hand although the bottom sediments may not be. That is, we are dealing only with the top 10 meters or so of sediment which may be somewhat variable.

In working with active sonar problems we usually use ray theory as shown in Fig. 1. The sound field is made up of contributions of rays that travel from the source to the receiver. On the right hand side of Fig. 1 we show two neighboring rays that bracket the receiver at range r. Thus there is an eigen-ray somewhere between these that travels precisely from the source to the receiver. Call this the n^{th} eigen-ray. The magnitude of the ray is A_n and its phase is θ_n. In the equations the terms that are not defined in the figure are R the reflection coefficient, ω the angular frequency, v the sound speed, $d\ell$ a path length along the ray, and m is the number of times the ray has touched a caustic. It is clear that the sediments interact with the sound field through the bottom reflection coefficient R, which is a complex number. The pressure carried by the ray is reduced by a factor equal to the modulus of R and the phase of the ray is advanced by the argument of R. In experimental work we can measure A_n and then determine $|R|$ from the equation for A_n.

In this paper we define R to be the plane wave reflection coefficient. As a matter of academic interest it could be argued that we should really be using a spherical reflection coefficient. This matter is discussed in Appendix A of the written paper. It is sufficient to say here that at high

frequencies the plane and spherical coefficients are essentially equal. At low frequencies the ray theory breaks down and we cannot separate the sound into packets that have a well defined trajectory. As shown in Appendix A we can write the direct and bottom reflected sound field at any frequency in terms of the plane wave reflection coefficient R.

The normal mode form of the wave theory representation, required for low frequency calculations, is shown in Fig. 2, (Bucker, 1970). The source is at depth z_0 and range zero and the receiver is at depth z and range r. The depth function U is a sum of linearly independent solutions of the z-separated part of the wave equation and k is the horizontal wave number. The k_n are those values of k for which U satisfies the boundary conditions. Consider the water near the bottom to have a constant sound speed v_b. Then the z-component solution for the layer can be written as a down-going plane wave $\exp(i\ell_b z)$ and an up-going plane wave $\exp(-i\ell_b z)$ multiplied by the plane wave reflection coefficient R. Small ℓ sub b, ℓ_b, is the vertical wave number. We can find the values of the coefficients A and B by requiring the usual interface conditions at depth z_p. These are that the pressure ($\rho\partial U/\partial t$) and the vertical component of particle velocity ($\partial U/\partial z$) must be continuous functions. We solve these two equations and take the limit $z_p \to z_b$ to obtain the values of A and B shown in Fig. 3. Note that the iso-speed layer has been removed from the problem as $z_p \to z_b$. However R remains in the solution in A and B.

Before proceeding to the models it should be noted that when working with active sonar systems we are sometimes interested in transient phenomena and need to know the time dependent response of the bottom. We will not cover these topics at this time but refer you to the excellent series of

papers by Ole Hastrup (Hastrup, 1966a, 1966b, 1968, 1969, 1970; Hastrup and Schunk, 1967) here at SACLANTCENTER. We will concentrate on plane wave sinusoidal solutions. Of course spherical waves can be formed by superposition of plane waves, and transient signals can be made up of sinusoidal signals.

II. PLANE WAVE REFLECTION COEFFICIENTS

A. Liquid

The most simple model of the bottom sediments is the Rayleigh model (Officer, 1958). The sediments are replaced by a liquid half-space. In Fig. 4 we have a velocity potential function $\phi(z_1)$, $-\infty < z_1 \leq 0$, that is the sum of a down-going plane wave $\exp i(\ell_0 z_1 + kx - \omega t)$ and a reflected up-going plane wave $R \exp i(-\ell_0 z_1 + kx - \omega t)$. Here k is the horizontal wave number, $k = (\omega/v_0) \cos \gamma_0$, where ω is the angular frequency, v_0 is the sound speed in the water half-space, and γ_0 is the grazing angle of the incident and reflected wave. Also, ℓ_0 is the vertical wave number, $\ell_0 = (\omega/v_0) \sin \gamma_0$, and R is the plane wave reflection coefficient. In the sediment half-space the velocity potential function $\phi(z_1)$, $0 \leq z_1 < \infty$ represents a down-going wave $T \exp i(\ell_1 z_1 + kx - \omega t)$. Here T is the transmission coefficient and ℓ_1 is defined by the equation $\ell_1^2 = (\omega/v_1)^2 - k^2$, where v_1 is the sound speed in the sediment half-space. In order to satisfy the Summerfeld radiation condition ℓ_1 is taken as the root of ℓ_1^2 that lies in the first quadrant of the complex plane.

We can now calculate R, and T if desired, by requiring that the sound pressure (equal to $\rho(\partial\phi/\partial t)$, where ρ is the density) and the vertical component of particle velocity (equal to $\partial\phi/\partial z$) be continuous across the interface at $z_1 = 0$. Solving these two equations for R results in the familiar Rayleigh reflection coefficient.

$$R = (\rho_1 \ell_0 - \rho_0 \ell_1)/(\rho_1 \ell_0 + \rho_0 \ell_1) \quad ,$$

where ρ_0 and ρ_1 are the density in the water half-space and in the sediment half-space respectively.

If sediment sound speed is greater than the water sound speed then there will be no bottom loss, i.e. mod(R) = 1, for grazing angles less than or equal to the critical angle γ_{0C} which is defined by the equation $\cos \gamma_{0C} = v_0/v_1$. As γ_0 varies from 0 to γ_{0C} the phase shift changes from -180° to 0° as shown in Fig. 5 where we have plotted the modulus of R, the phase shift (i.e. the argument of R), and bottom-loss (i.e. - 20 $\log_{10}$ [mod(R)]) as a function of grazing angle. The example corresponds to coarse sand from the continental terrace in Hamilton's tables (Hamilton, 1974a). The value of v_1/v_0 is 1.201, corresponding to a critical angle of 33.6°, and the value of ρ_1/ρ_0 is 2.034.

If the sediment sound speed is less than the water sound speed then the losses are much higher for the small grazing angles. At the angle of intromission γ_{0I}, which is defined by the equation

$$\cos^2\gamma_0 = [(\rho_0 v_0)^2 - (\rho_1 v_1)^2]/[(\rho_0 v_1)^2 - (\rho_1 v_1)^2]$$

R is zero, or all sound energy is transmitted into the sediment half-space. The phase shift is -180° for $\gamma_0 < \gamma_{0I}$ shifting abruptly to 0° for $\gamma_0 > \gamma_{0I}$. Fry and Raitt (Fry and Raitt, 1961) measured this phase shift for deep sea Pacific sediments and by using known values of the density were able to determine the sound speed of the near bottom sediments.

Figure 6 shows the values of mod(R), phase shift, and bottom loss for low speed bottom corresponding to silty-clay from a continental terrace. The sediment-water sound speed ratio is 0.994 and the sediment-water density ratio is 1.421. These set the angle of intermission at 6.3°.

The effect of sediment attenuation can be introduced into the model (Mackenzie, 1960) by modifying the equation for ℓ_1^2 as follows

$$\ell_1^2 = [(\omega/v_1) + i\alpha_1/8.686]^2 - k^2 \quad ,$$

where α_1 is the attenuation of the sound wave in the sediment in dB per unit length. In Fig. 7 we have plotted the bottom loss as a function of γ_0 for the case where the sediment sound speed is greater than the water speed for several values of α_1. Hamilton (1972, 1974) has derived a simple empirical formula that relates a to sediment porosity and frequency.

Figure 8 shows the effect of increasing absorption for the low speed bottom. The essential effect is the removal of the peak in the bottom loss curve at the angle of intermission.

B. Solid

The liquid model of the bottom may be used in crude calculations, however, we do know that sediments have rigidity and we must account for this in accurate calculations. An isotropic sediment layer can be described by three sediment parameters (as shown in Fig. 9), the density ρ and the two Lamé constants lambda and mu, (Ewing, Jardetsky, and Press, 1957). The density can be measured directly but lambda and mu are determined by the speed and attenuation of the compressional and shear waves that travel in the sediment. These are related by two equations (Bucker et. al., 1965)

$$(\lambda + 2\mu) = \rho(x_p^2 - y_p^2 - i\,2x_p\,y_p)/(x_p^2 + y_p^2)^2$$

$$\mu = \rho(x_s^2 - y_s^2 - i\,2x_s\,y_s)/(x_s^2 + y_s^2)^2 \quad .$$

Here λ and μ are the Lamé constants, ρ is the density, $x_p = 1.0/v_p$, $y_p = \alpha_p/(8.686\ \omega)$, $x_s = 1.0/v_s$, $y_s = \alpha_s/(8.686\ \omega)$, v_p and v_s are sound speeds of the compressional wave and the shear wave respectively, and α_p and α_s are the attenuation (in dB per unit length) of the compressional and shear waves. Given v_p, v_s, α_p and α_s we can solve directly for λ and μ. If we do not know α_s then we can use the v_p, v_s and α_p and the assumption of zero volume viscosity (i.e. $Im(\lambda) + (2/3)Im(\mu) = 0$) to solve for λ and μ. If we do not know either v_s or α_s then we assume zero volume viscosity and an estimate of the rigidity (we define rigidity = $r = Re(\mu)/Re(\lambda)$) and then solve for λ and μ. Reflection of a plane wave from a solid half-space is shown in Fig. 10. A plane compressional wave is incident on the interface at grazing angle γ_0. There is a reflected wave in the water and a compressional wave and a vertically polarized shear wave in the solid. Note that there has been a simple change in notation to conform with geophysical publications. Earlier we formulated the problem in terms of the horizontal wave number k and the vertical wave number ℓ. Now the problems use the horizontal phase velocity $c(c = \omega/k)$ and the parameter r_α which is equal to ℓ divided by k. To solve for the three unknowns, R, T_p, and T_s, we require the following three interface conditions: (i) continuity of pressure, (ii) continuity of vertical particle motion, and (iii) zero stress on the x direction on the solid by the water. Solution of the interface equations results in the well known expression for R

$$R = (q-1)/(q+1) ,$$

where

$$q = \rho_1 r_{\alpha 0} [(\gamma_1 - 1)^2 + \gamma_1 r_{\beta 1} r_{\alpha 1}]/(\rho_0 r_{\alpha 1}) .$$

Here ρ_0 and ρ_1 are the density of the water and the solid respectively and the other quantities are defined as

$$r_{\alpha 0} = [(c/v_0)^2 - 1]^{1/2} ,$$

$$r_{\alpha 1} = [\rho_1 c^2/(\lambda_1 + 2\mu_1) - 1]^{1/2} ,$$

$$r_{\beta 1} = [\rho_1 c^2/\mu_1 - 1]^{1/2} ,$$

$$\gamma_1 = 2\mu_1/(\rho_1 c^2) , \text{ and } c = \omega/k .$$

Roots are chosen so that $r_{\alpha 0}$, $r_{\alpha 1}$, and $r_{\beta 1}$ lie in the first quadrant of the complex plane.

In Fig. 11 we have plotted bottom loss, phase, and the modulus of R as a function of grazing angle. For the case shown the ratios ρ_1/ρ_0, v_{r1}/v_0, and v_{s1}/v_0 are 2.6, 4.46 and 2.57 respectively. The rigidity value, r, is equal to 1.0. For all practical purposes the bottom loss is essentially zero. There are two critical angles. The first, γ_{cs}, comes when the horizontal phase velocity is equal to the shear speed. There are no losses for grazing angles less than γ_{cs}. The second critical angle, γ_{cp}, occurs when the phase velocity is equal to the compressional sound speed.

C. Multi-Layer Liquid

We next want to consider multi-layered sediment models that can be used either to represent actual layering (e.g. it is not uncommon to find alternating layers of sand and silt in shallow water) or to account for

gradients. For the layered liquid case the solution is very simple. In Fig. 12 we have n sediment layers and a half-space labeled (n + 1). In each layer the potential function is the sum of an up- and a down-going plane wave (e.g. ϕ_n - $A_n \exp(i \ell_n z_n) + B_n \exp(-i \ell_n z_n)$) and in the half-space the potential function represents a down-going wave ($\phi_{n+1} = \exp(i \ell_{n+1} z_{n+1})$). If we let P represent the pressure ($P = \rho\phi$) and Q the vertical component of particle velocity we can start at the interface between layer n and the half-space with the values of P and Q as shown at the top of Fig. 13. P, equal to $\rho\phi$, and Q, equal to $d\phi/dz$ are easily evaluated at the n/(n+1) interface where z_{n+1} is zero. Because P and Q are continuous functions they have the same values at the bottom of layer n (at $z_n = d_n$) that they have at the top of the half-space (at $z_{n+1} = 0$). Therefore we can calculate A_n and B_n as shown in Fig. 13 and from these calculate P and Q at the top of layer n (at $z_n = 0$). We continue working up the layers until we have values for A_0 and B_0 from which the value of R is obtained, $R = B_0/A_0$.

D. Multi-Layer Linear Gradient

We consider now another method for modeling the change of sediment properties with depth due to increasing compaction and temperature. In this approach we account for changes in sound speed and density by using single or multiple liquid layers where Airy functions can be used to represent the sound energy. This method has been used by Morris (Morris, 1970) and also by Hanna (Hanna, 1973) to explain low values of bottom loss at small grazing angles and low frequency. In this case we will use a somewhat different function χ as shown at the top of Fig. 14. The general wave equation for the case where there is variation in both sound speed

and density is shown on the second line (Brekhovskikh, 1960). Cap. K squared is defined on the third line. If cap. K squared can be represented as a linear function of depth then the potential function χ can be written as the sum of the Airy functions Ai and Bi. The argument of the Airy functions is defined in terms of the horizontal wave number k, the profile parameters K_0 and β and the depth z by the relation shown in the 6th line. To add the effect of absorption in the liquid an imaginary term $i\alpha/8.686$ is added to K_0 as shown on the bottom line.

A multi-layered model composed of linear K^2 and constant K (constant sound speed) layers is shown in Fig. 15. We can start at the bottom, and work up through the layers using the interface conditions that the pressure and the vertical component of particle velocity are continuous functions. In this case P, equal to the pressure, is $\sqrt{\rho}\chi$ and Q, equal to $-i\omega$ times the particle velocity, is $\rho^{-1}\, d(\sqrt{\rho}\chi)/dz$. Note that in Fig. 15 we have made layer 2 a constant K layer. The ability to mix linear and constant layers is necessary in a general program because as the gradient, β, goes to zero the argument of the Airy functions increases without limit. Thus depending on frequency, layer thickness, and computer word length there is a minimum gradient that can be used. Layers with gradients smaller than this must be represented by constant K layers.

Now that we have two models that account for gradients it will be instructive to see how they compare. To do this consider Fig. 16. On the left hand side our linear model has a sound speed that increases from 1500 m/sec at the water/sediment interface to 1800 m/sec at a sediment depth of 300 m which corresponds to an average sound speed

gradient equal to (1800 - 1500) m/sec ÷ 300 m, or 1 sec^{-1}. The constant K model is shown for two layers. The layers have the same thickness and the sound speed at the center of the layers (i.e. at 75 and 225 m) is set equal to the sound speed of the linear layer at that depth.

On the right hand side of Fig. 16 is a diagram that indicates the main physical events. Most of the energy either reflects at the surface or is refracted in the sediment because of the gradient. Morris (Morris, 1973) has used a ray description to calculate the energy in each path and compare the ray description with the wave model. Of course there are 2nd and higher order effects as indicated by the dashed arrows that are implicit in the wave model.

In Fig. 17 we show our first comparison of the two models. For the calculations we used a frequency of 100 Hz, a density ratio (ρ in sediment)/(ρ in water) equal to 2.0, and zero attenuation. The reflection coefficient was calculated for grazing angles from 0° to 20° which are of interest in sound propagation. With zero attenuation both models return all sound to the water for these grazing angles so the modulus of R is 1.0 or the bottom loss is zero. Figure 17 shows plots of phase, i.e. the argument of R, for different cases. The curve marked L is for the linear K^2 model, while the curves labeled 1, 3, or 10 correspond to 1, 3, or 10 constant K layers. The 10 layer case has a layer thickness of 30 m which is equal to 2 wavelengths in the water. For 30 layers (or a thickness of 0.67 λ_w) there is a maximum phase difference of 2.2° at a grazing angle of 3.5° which cannot be plotted on this scale. For 100 layers there is a maximum phase difference of 0.2°.

In Fig. 18 we are using the same models except that there is an attenuation of 0.05 dB/m in both models. As in the previous case the 10 layer model (thickness = 2 λ_{ω}) has a maximum difference of ~10° and the 30 layer model has essentially the phase as the linear model. It is interesting to note that the attenuation has slowed the phase change a considerable amount. This will have a noticeable effect on the wave theory propagation models where a shift in phase of 360° will add a new mode to the sound field. (Bucker, 1964).

To complete the comparison of the linear and constant layers, the bottom loss curves are shown in Fig. 19. The one layer case has much less bottom loss because the sound speed is equal to the sound speed of the linear model at 150 m depth which is 1629.6 m/sec and corresponds to a critical angle greater than 20°.

E. Multi-Layer Solid

There are several approaches to the problem of modeling the sediment layers when there are significant changes of the sediment properties with depth. Gupta (1966a, 1966b) has developed closed solutions for the case where the compressional and shear velocity varies linearly with depth while the density remains constant. More general variations can be treated with the propagator method developed by Gilbert and Backus (1966). One problem of the propagator method is loss of accuracy when sediment penetration of many wavelengths occurs. In the most recent programs at NUC we have chosen to model the variable sediment properties with many layers and to maintain accuracy by use of Knopoff's formulation (Knopoff, 1964).

The multi-layer solid model is substantially more difficult than the multi-layer liquid model for two reasons. First there are twice as many waves (shear waves as well as compressional waves) and twice as many interface conditions (continuity of horizontal components of stress and strain as well as continuity of vertical components of stress and strain). Second you cannot start at the bottom and work to the top. All of the layers have to be considered as a group. The situation is shown in Fig. 20. There are an up- and a down-going compressional wave in the water, an up- and a down-going compressional wave and an up- and a down-going shear wave in each solid layer, and down-going compressional and shear waves in the bottom half-space. We can arbitrarily set the coefficient $A_{n+1} = 1$, as shown, so that there are $4n + 3$ unknown coefficients (A_0, B_0, A_1, B_1, C_1,..., C_{n+1}), where n is the number of layers. There are also $4n + 3$ interface conditions. Three conditions at the first interface (continuity of vertical components of stress and strain and zero horizontal stress) and four conditions at all other interfaces (continuity of vertical and horizontal stress and strain). Since the interface conditions can be written as a set of linear homogeneous algebraic equations the solution can be done using standard matrix inversion algorithms. This is not a practical method of solution when n is large because we would have to invert a matrix of $(4n + 3)^2$ elements and because of loss of accuracy problems. The number of terms in the problem can be kept under control by using transfer matrices that transfer the stress and strain at one interface of a layer to the other interface. This method was developed by Thomson (1950). For the problem of sound transmission through plates and extended by Bucker,

Whitney, Yee, and Gardner (1965) to include wave attenuation for the problem of bottom reflection. A serious drawback of the transfer matrix method is that it also suffers from loss of accuracy problems.

Fortunately the accuracy problems can be solved using methods developed by the geophysicists for earthquake problems (Thrower, 1965; Dunkin, 1965; Watson, 1970; Schwab, 1970). This is discussed in Appendix B. The results are summarized in Fig. 21. For a layered structure of the same form that we have for the bottom reflection problem there are natural vibrations at frequencies corresponding to zeroes of a determinant, $|\Delta_R|$, called the Rayleigh determinant. The geophysicists have developed very fast and accurate methods for calculating $|\Delta_R|$. In Appendix B we show that the reflection coefficient can be written as $R = (\rho_1 r_{\alpha 0} |\Delta_R| - \rho_0 |\Delta_S|)/(\rho_1 r_{\alpha 0} |\Delta_R| + \rho_0 |\Delta_S|)$ where $|\Delta_S|$ is the same as $|\Delta_R|$ except for row 1. Thus we can use the sophisticated methods of the geophysicists to solve our problem. We do have to generalize the equations to account for attenuation which is neglected at earthquake frequencies.

Figure 22 is a plot of bottom loss for a model of 100 layers. The curve labeled L is for the liquid layer model (it is also the bottom loss curve for the linear model). The other curves are for a 100 layer solid model with different values of rigidity. For r = 0 the curve is quite similar to the liquid model except that there is slightly more loss due to some conversion of compressional waves into shear waves. As the rigidity increases there are lower losses than the liquid model at very small grazing, angles and higher losses than the liquid model at larger grazing angles. Most likely the propagation to long ranges would be better for the r = 0.1 curve than for the liquid model.

III. COMPARISON WITH EXPERIMENT

The U.S. Navy has been concerned about the operation of bottom bounce sonars over the last twenty years. It is therefore not surprising that there have been a large number of laboratory reports on bottom loss, many of which are classified.

At the Underwater Sound Laboratory in New London (now NUSC-NL) the research work has concentrated on problems associated with the SQS-26 sonar. Significant papers have been published by Karamargin (1962), Cole (1965), Menotti, Santaniello, and Schumacher (1965).

At the Naval Undersea Center at San Diego most of the work has centered on data collected during three FASOR (forward area sonar research) cruises. Data was collected in over 90 stretegic areas in the Western Pacific Ocean, in contiguous seas and basins, and in the Indian Ocean. Most of the journal reports have been written by Hamilton (on sediment properties, (Hamilton, 1974a, b) and by Bucker and Morris (on calculation of the plane wave reflection coefficient, (Bucker et.al., 1965; Morris, 1970, 1973)).

At the Applied Research Laboratory (Univ. of Texas) sediment properties have been measured by Hampton (1967) and bottom reflection calculations have been reported by Banard, Bardin, and Hempkins (1964). Also, Frev (1967) has published a bibliography on the reflection and scattering of sound from the ocean bottom.

At SACLANTCEN the work of Hastrup has been already cited. More recently there have been significant reports by Tuncay Akal (1972, 1974).

We will illustrate the agreement between experimental data and calculated values of bottom loss with some NUC data from the FASOR cruises. In

the first case, Fig. 23, data is from an abyssal hill province in the Northeast Pacific and the frequency is 1.6 kHz. Two calculated curves are shown, one with a gradient and one with constant sound speed. The gradient model provides a somewhat better fit but there is not a large difference between the two. In the next figure, Fig. 24, the frequency has been reduced to 200 Hz and it is clear that there is refracted energy responsible for the small values of bottom loss that is not included in the iso-speed model.

Our last example, Fig. 25, is from the Coral Sea. The frequency is 50 Hz. At the lower grazing angles we see some negative bottom losses in the experimental data. This could be due to an error in the assummed source level of the explosive charges or some inacurracy in the analysis. We feel that a more fundamental problem is in doing an analysis of 50 Hz bottom loss. At very low frequencies we are concerned with passive systems which process essentially CW signals. Also the received signal is made up of all possible paths that can travel from the source to the receiver. The performance of operational systems can be accurately simulated with a CW source. The measured results can then be compared to wave theory calculations involving plane wave reflection coefficients as discussed before. It should be easy to determine the sensitivity of the acoustic field to bottom interaction and the accuracy of the reflection coefficient. By introducing the bottom loss measurements with the explosive charges we have unnecessarily complicated our analysis problem.

IV. SUMMARY

We began this review with the ray theory equations and the problem of a bottom bounce sonar. As far as levels are concerned this problem is mostly solved. With a good description of the upper 10 m or so of sediments a reflection coefficient can be calculated, converted to bottom loss and used in a ray theory description of the sound field. There are probably cases where the bottom is so rough that this direct approach is not applicable, but in the data that we have worked with, it does.

Several models of varying complexity for calculating the plane wave bottom reflection coefficient have been discussed. The most general model is composed of an almost unlimited number of solid layers with attenuation and should represent any reasonably uniform sediment structure.

At lower frequencies (e.g. below 2 kHz) we begin to see an appreciable amount of energy that is refracted from the positive gradients in the sediments. The sediment parameters must be defined to a depth at least as deep as the refracting sound field. This requires several hundred meters of sediment data. Also at the lower frequencies the formalism of ray theory begins to break down as the bottom and direct wave fronts begin to interact. We suggest that at low frequencies the standard shot runs and bottom loss curves are not useful and that we should consider CW experiments where the total sound field is measured and compared to wave theory calculations that contain bottom interaction in the plane wave reflection coefficient.

V. REFERENCES

Tuncay Akal, "Acoustical Characteristics of the Sea Floor: Experimental Techniques and Some Examples from the Mediterranean Sea", in Physics of Sound in Marine Sediments, pp. 447-480, Ed. by Loyd Hampton, Plenum Press, New York (1974).

Tuncay Akal, "The Relationship Between the Physical Properties of Underwater Sediments that Affect Bottom Reflection", Marine Geology 13, 251-266 (1972).

G. R. Barnard, J. L. Bardin, and W. B. Hempkins, "Underwater Sound Reflection from Layered Media," J. Acoust. Soc. Am. 36, 2119-2123 (1964).

Leonid M. Brekhovskikh, Waves in Layered Media, p. 171, English Translation, Academic Press, New York (1960).

H. P. Bucker, "Normal Mode Propagation in Shallow Water," J. Acoust. Soc. Am. 36, 251-258 (1964).

H. P. Bucker, J. A. Whitney, G. S. Yee and R. R. Gardner, "Reflection of Low Frequency Sonar Signals from a Smooth Ocean Bottom," J. Acoust. Soc. Am. 37, 1037-1051 (1965).

H. P. Bucker, "Sound Propagation in a Channel with Lossy Boundaries," J. Acoust. Soc. Am. 48, 1187-1194 (1970).

B. F. Cole, "Marine Sediment Attenuation and Ocean Bottom Reflected Sound," J. Acoust. Soc. Am. 38, 291-297 (1965).

J. W. Dunkin, "Computation of Modal Solutions in Layered Elastic Media at High Frequencies," Bull. Seism. Soc. Am. 55, 335-358 (1965).

W. Maurice Ewing, Wenceslas S. Jardetsky and Frank Press, Elastic Waves in Layered Media, pp. 79-83, McGraw-Hill Book Co., New York (1957).

H. G. Frey, "Reflection and Scattering of Sound by the Ocean Boundaries: A Bibliography," Defense Research Lab, Acoust. Report No. 285.

John C. Fry and Russell W. Raitt, "Sound Velocities at the Surface of Deep Sea Sediments," J. Geophys. Res. 66, 589-597 (1961).

Freeman Gilbert and George E. Backus, "Propagator Matrices in Elastic Wave and Vibration Problems," Geophysics 31, 326-332 (1966).

Ravindra N. Gupta, "Reflection of Sound Waves from Transition Layers," J. Acoust. Soc. Am. 39, 255-260 (1966a).

Ravindra N. Gupta, "Reflection of Elastic Waves from a Linear Transition Layer," Bull. Seism. Soc. Am. 56, 511-526 (1966b).

E. L. Hamilton, "Compressional Wave Attenuation in Marine Sediments," Geophysics 37, 620-646 (1972).

E. L. Hamilton, "Prediction of Deep-Sea Sediment Properties: State of the Art," pp. 1-43 in Deep Sea Sediments, Physical and Mechanical Properties, Ed. by A. L. Interbitzen, Plenum Press (1974a).

E. L. Hamilton, "Geoacoustic Models of the Sea Floor," pp. 1-43, in Physics of Sound in Marine Sediments, Ed. by L. Hampton, Plenum Press, (1974b).

L. D. Hampton, "Acoustic Properties of Sediments," J. Acoust. Soc. Am. 42, 882-890 (1967).

K. V. Mackenzie, "Reflection of Sound from Coastal Bottoms," J. Acoust. Soc. Am. 32, 221-231 (1960).

F. R. Menotti, S. R. Santaniello and W. R. Schumacher, "Studies of Observed and Predicted Values of Bottom Reflectivity as a Function of Incident Angle," J. Acoust. Soc. Am. 68, 707-714 (1965).

Halcyon E. Morris, "Bottom Reflection Loss Model with a Velocity Gradient," J. Acoust. Soc. Am. 48, 1198-1202 (1970).

Halcyon E. Morris, "Ray and Wave Solutions for Bottom Reflection for Linear Sediment Layers," J. Acoust. Soc. Am. 53, 323(A) (1973).

C. B. Officer, Introduction to the Theory of Sound Transmission with Application to the Ocean, pp. 74-82, McGraw Hill Book Co., New York (1958).

Fred Schwab, "Surface-Wave Dispersion Computations: Knopoff's Method," Bull. Seism. Soc. Am. 60, 1491-1520 (1970).

W. T. Thomson, "Transmission of Elastic Waves Through a Stratified Solid Medium," J. Appl. Physics 21, 89-93 (1950).

E. N. Thrower, "The Computation of Dispersion of Elastic Waves in Layered Media," J. Sound Vib. 2, 210-226 (1965).

T. H. Watson, "A Note on Fast Computation of Rayleigh Wave Dispersion in the Multilayered Half-Space," Bull. Seism. Soc. Am. 60, 161-166 (1970).

$$\Psi = \sum_n A_n \exp(i\Theta_n)$$

$$A_n = |R| \left[\cos\gamma_s \, \delta\gamma_s / (r\,\delta h)\right]^{1/2}$$

$$\Theta_n = \int_0^r \frac{\omega}{v} d\ell + \mathrm{ARG}(R) - \frac{m\pi}{2}$$

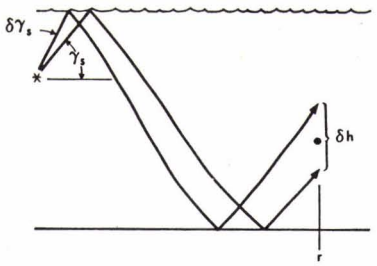

FIG. 1 RAY THEORY REPRESENTATION (HIGH FREQUENCY)

$$\Psi = \left(\frac{2\pi}{r}\right)^{1/2} \sum_n U_n(Z_o)\, U_n(Z)\, e^{ik_n r}$$

$$U = A\, f(Z) + B\, g(Z), \quad 0 \le Z \le Z_p$$

$$U = \exp\left[i\ell_b Z\right] + R \exp\left[i\ell_b (2Z_b - Z)\right]$$

$$(Z_p < Z < Z_b)$$

$$\ell_b^2 = (\omega/v_b)^2 - k^2$$

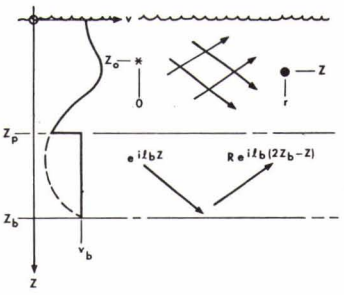

FIG. 2 WAVE THEORY REPRESENTATION (LOW FREQUENCY)

INTERFACE CONDITIONS

CONTINUITY OF PRESSURE (ρU)

CONTINUITY OF VERTICAL COMPONENT OF PARTICLE VELOCITY $\left(-\frac{\partial U}{\partial z}\right)$

SOLVE FOR A AND B AS $z_p \rightarrow z_b$

$$A = \exp(i\ell_b Z_b)\left[g'_b (1+R) - i\ell_b g_b (1-R)\right]/W.$$

$$B = \exp(i\ell_b Z_b)\left[i\ell_b f_b (1-R) - f'_b (1+R)\right]/W.$$

WHERE, $W = f_b g'_b - f'_b g_b$.

$f_b = f(Z_b)$, $g_b = g(Z_b)$, $f'_b = (df/dZ)_{Z_b}$, $g'_b = (df/dZ)_{Z_b}$

FIG. 3 INTRODUCTION OF R INTO WAVE SOLUTIONS

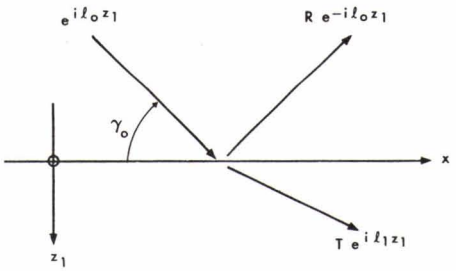

$$k = (\omega/v_o)\cos\gamma_o, \quad \ell = (\omega/v_o)\sin\gamma_o$$

$$\ell_1^2 = (\omega/v_1)^2 - k^2$$

$$R = (\rho_1 \ell_o - \rho_o \ell_1) / (\rho_1 \ell_o + \rho_o \ell_1)$$

FIG. 4 REFLECTION FROM LIQUID–LIQUID INTERFACE (RAYLEIGH MODEL)

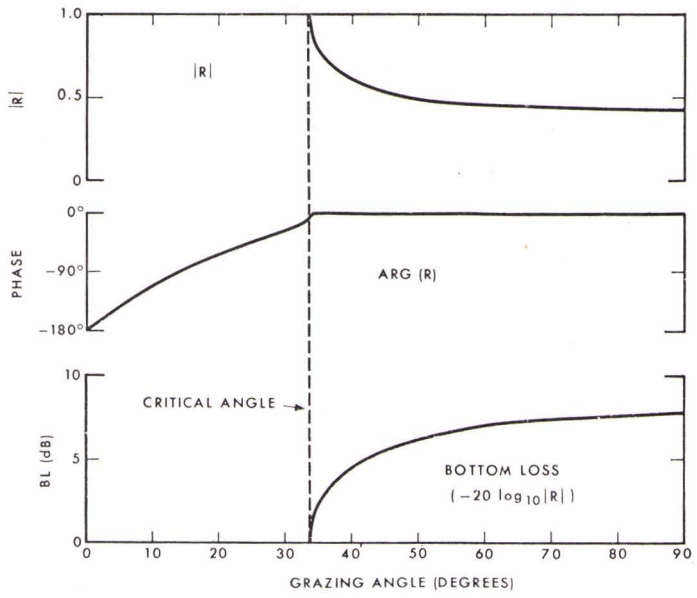

FIG. 5
RAYLEIGH MODEL ($v_1 > v_o$)

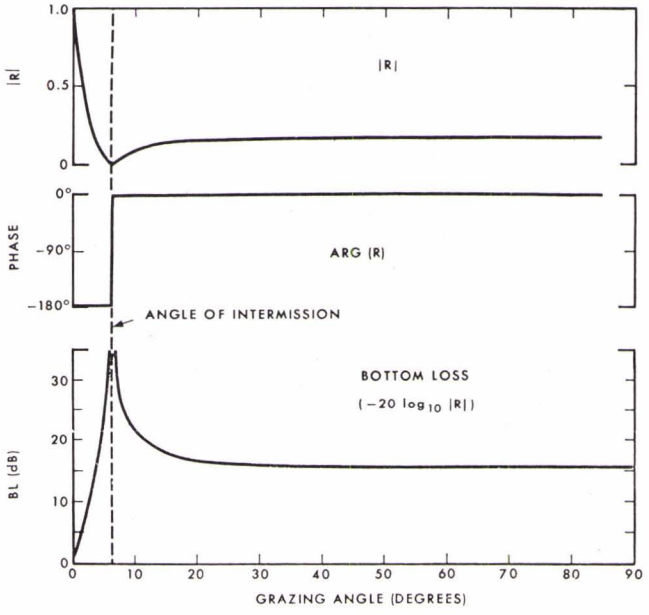

FIG. 6
RAYLEIGH MODEL ($v_1 < v_o$)

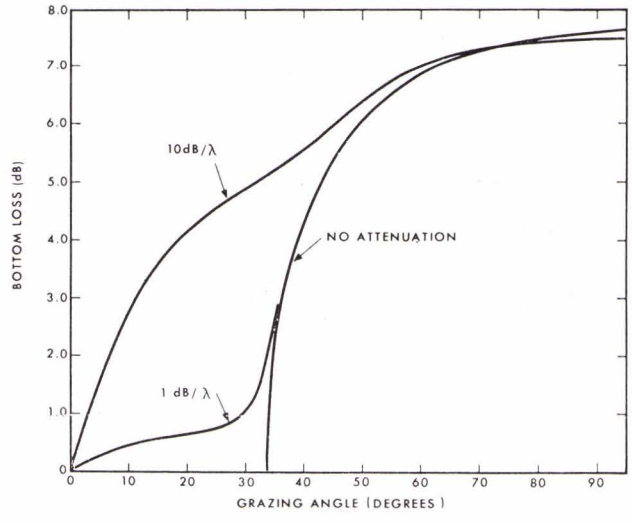

FIG. 7
RAYLEIGH MODEL ($v_1 > v_o$)
FOR 0, 1, 10 dB/λ ATTENUATION

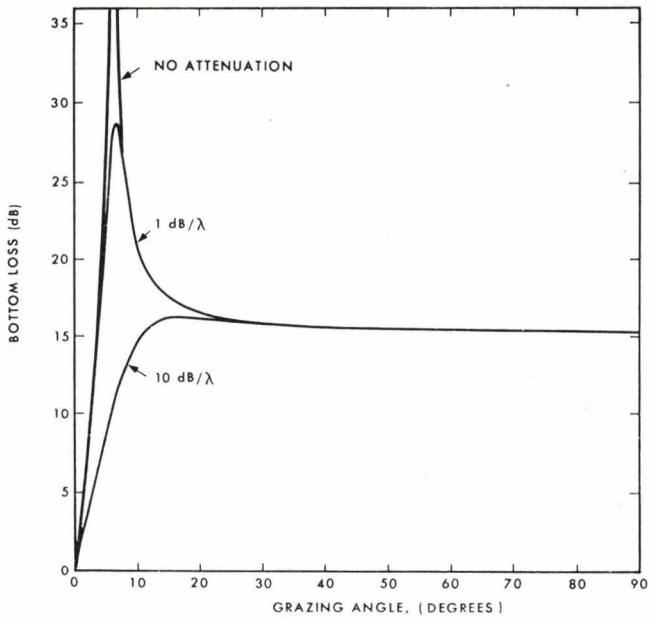

FIG. 8
RAYLEIGH MODEL ($v_1 < v_o$)
FOR 0, 1, 10 dB/λ ATTENUATION

SEDIMENT PARAMETERS ρ, $\underbrace{\lambda, \mu}_{\text{LAMÉ CONSTANTS}}$

ACOUSTIC PARAMETERS

v_p = SOUND SPEED (COMP. WAVE)

v_s = SOUND SPEED (SHEAR WAVE)

a_p = ATTEN., dB/UNIT LENGTH (COMP.)

a_s = ATTEN., dB/UNIT LENGTH (SHEAR)

CONSTITUTIVE EQUATIONS

$$\lambda + 2\mu = \rho(x_p^2 - y_p^2 - i2x_p y_p)/(x_p^2 + y_p^2)^2$$

$$\mu = \rho(x_s^2 - y_s^2 - i2x_s y_s)/(x_s^2 + y_s^2)^2$$

NOTATION

$x_p = 1/v_p$, $y_p = a_p/(8.686\omega)$

$x_s = 1/v_s$, $y_s = a_s/(8.686\omega)$

FIG. 9
SEDIMENT AND ACOUSTIC PARAMETERS FOR SOLID

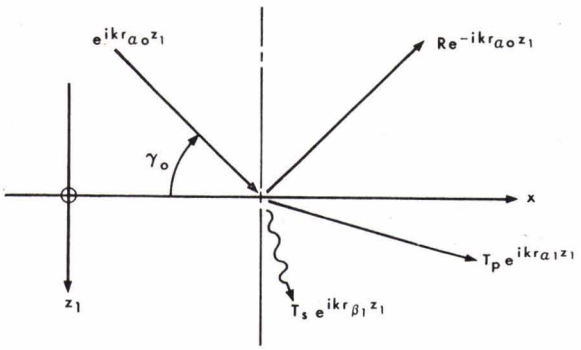

FIG. 10
REFLECTION FROM LIQUID–SOLID INTERFACE

$$R = (q-1)/(q+1)$$

WHERE $q = \rho_1 r_{ao}[(\gamma_1 - 1)^2 + \gamma_1 r_{\beta 1} r_{\alpha 1}]/(\rho_o r_{\alpha 1})$

$r_{ao} = \ell_o/k = [(c/v_o)^2 - 1]^{1/2}$

$r_{\alpha 1} = \ell_1/k = [\rho c^2/(\lambda + 2\mu) - 1]^{1/2}$

$r_{\beta 1} = [\rho c^2/\mu - 1]$

$\gamma_1 = 2\mu_1/(\rho_1 c^2)$

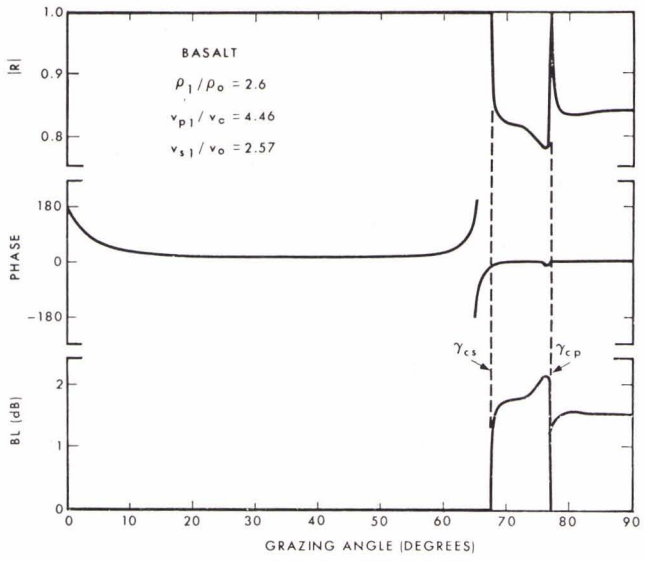

FIG. 11
REFLECTION FROM BASALT

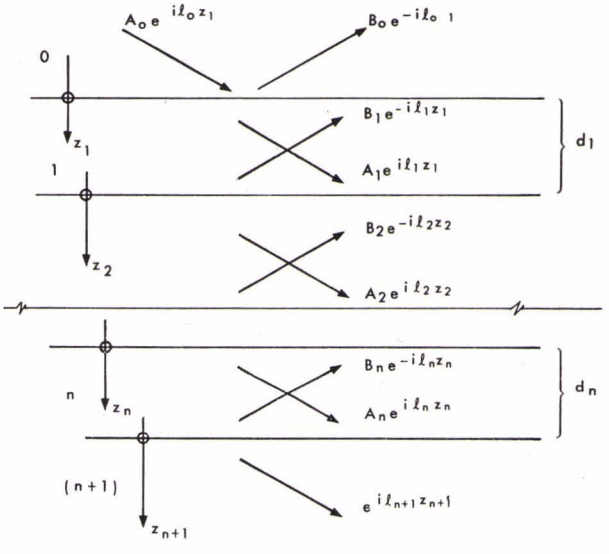

FIG. 12
MULTI-LAYER LIQUID MODEL

INTERFACE n/(n+1): $P = \rho\varphi = \rho_{n+1}$, $Q = (d\varphi/dz) = i\ell_{n+1}$

LAYER n:

$$A_n = \tfrac{1}{2}\exp(-i\ell_n d_n)\,[P/\rho_n + Q/(i\ell_n)]$$

$$B_n = \tfrac{1}{2}\exp(i\ell_n d_n)\,[P/\rho_n - Q/(i\ell_n)]$$

INTERFACE (n—1)/n:

$$P = \rho_n(A_n + B_n)$$

$$Q = i\ell_n(A_n - B_n)$$

CONTINUE UNTIL A_o & B_o ARE CALCULATED

REFLECTION COEFFICIENT: $R = B_o/A_o$

FIG. 13
CALCULATION OF R FOR MULTI-LAYER LIQUID

$$p = \sqrt{\rho}\,\chi$$

WAVE EQ. $\nabla^2 \chi + K^2 \chi = 0$

WHERE, $K^2 = (\omega/v)^2 + \frac{1}{2\rho}(d^2\rho/dz^2) - \frac{3}{4}\left[\frac{1}{\rho}(d\rho/dz)\right]^2$

IF $K^2 = K_o^2(1+\beta z)$

THEN $\chi = A \cdot Ai(\xi) + B\,Bi(\xi)$

WHERE $\xi = \frac{k^2 - K_o^2}{(K_o^2\beta)^{2/3}} - (K_o^2\beta)^{1/3} z$

TO ADD α (dB/UNIT LENGTH) ATTENUATION: $K_o \rightarrow K_o + i\frac{\alpha}{8.686}$

FIG. 14
WAVE SOLUTIONS FOR THE LINEAR MODEL

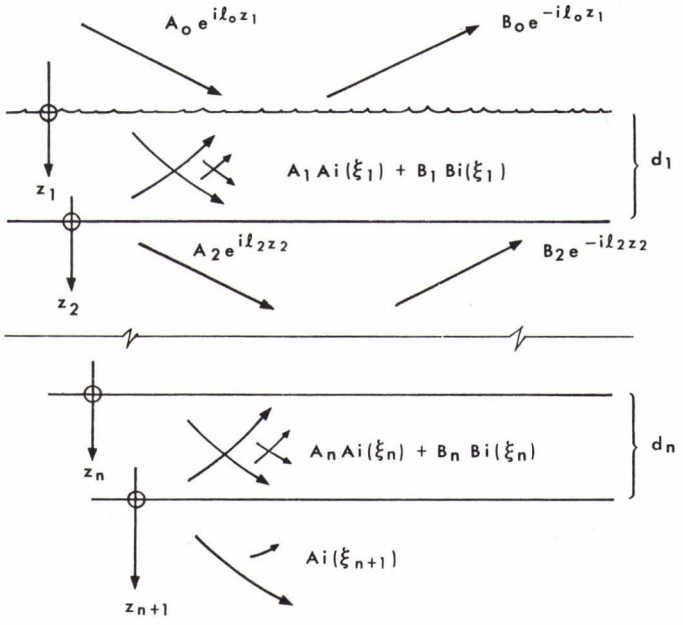

FIG. 15
MULTI-LAYER LINEAR LIQUID MODEL

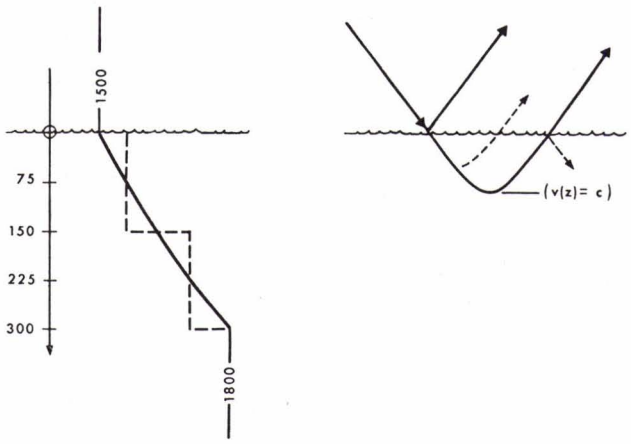

FIG. 16
LINEAR K^2 AND CONSTANT K LAYERS

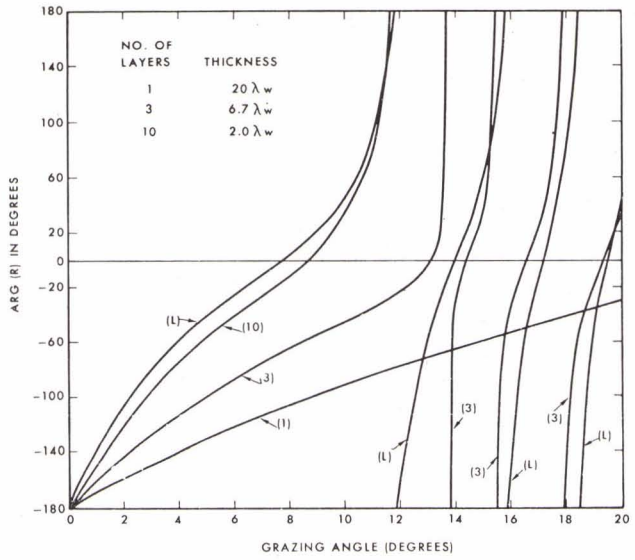

FIG. 17
PHASE COMPARISON FOR LINEAR K^2 AND CONSTANT K MODELS
(Zero Attenuation)

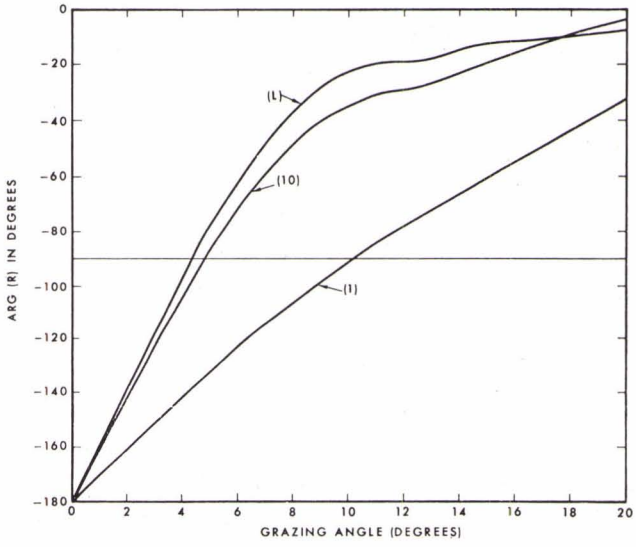

FIG. 18
PHASE COMPARISON FOR LINEAR K^2 AND CONSTANT K MODELS
(0.05 dB/m Attenuation)

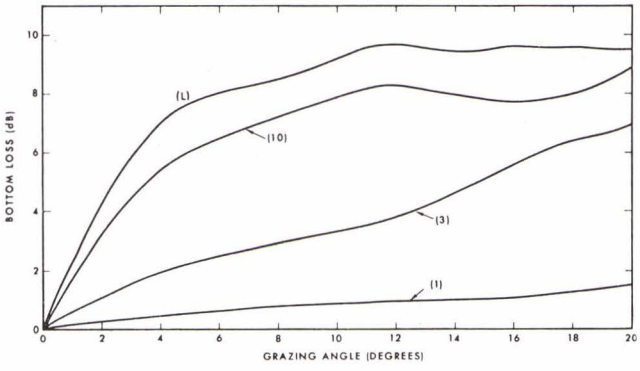

FIG. 19
BOTTOM LOSS COMPARISON FOR LINEAR K^2 AND CONSTANT K MODELS
(0.05 dB/m Attenuation)

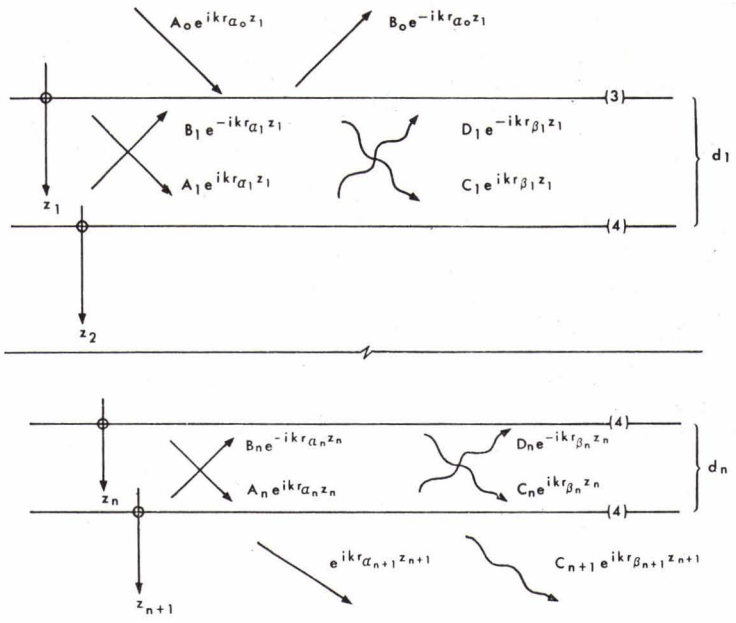

FIG. 20
MULTI-LAYER SOLID MODEL

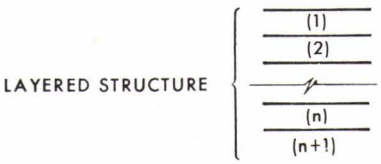

NATURAL VIBRATIONS (EARTHQUAKE WAVES) OCCUR AT ZERO'S OF RAYLEIGH DETERMINANT $|\Delta_R|$

WE CAN SHOW THAT $$R = \frac{\rho_1 r_{\alpha_o} |\Delta_R| - \rho_o |\Delta_S|}{\rho_1 r_{\alpha_o} |\Delta_R| + \rho_o |\Delta_S|}$$

WHERE Δ_S IS THE SAME AS Δ_R

EXCEPT FOR ROW 1

FIG. 21
REFLECTION COEFFICIENT FOR THE MULTI-LAYER SOLID MODEL

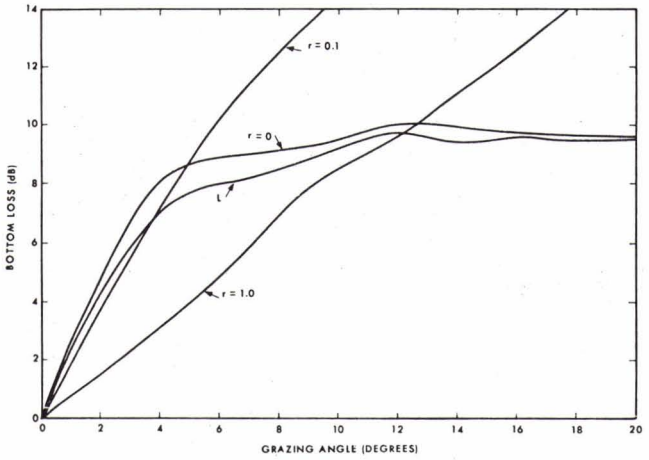

FIG. 22
COMPARISON OF MULTI-LAYER SOLID AND LIQUID MODELS

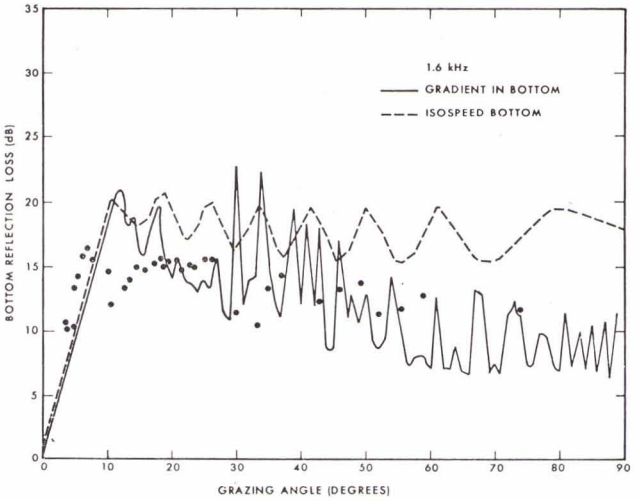

FIG. 23
COMPARISON OF GRADIENT AND NO GRADIENT MODELS WITH 1.6 kHz DATA

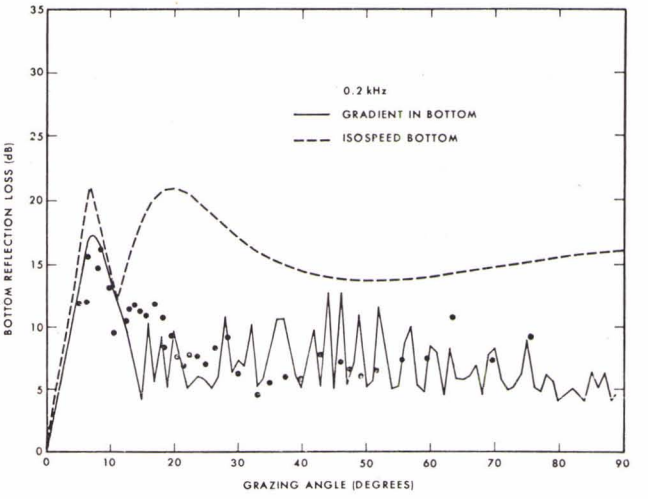

FIG. 24
COMPARISON OF GRADIENT AND NO GRADIENT MODELS WITH 0.2 kHz DATA

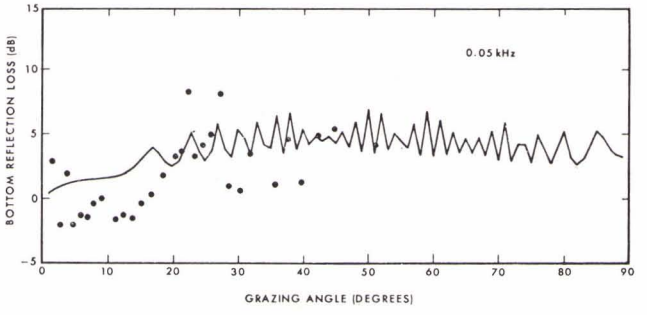

FIG. 25
COMPARISON OF GRADIENT MODEL WITH 0.05 kHz DATA

VII. APPENDICES

APPENDIX A: Formulation of the Sound Field Using the Plane Wave Reflection Coefficient R

The general form of the sound field can be written as a sum of cylindrical waves in the form (Bucker, 1970)

$$\psi = \int_0^\infty -2\, U(z_0)V(z)\, W^{-1}\, J_0(kr)\, kdk \qquad (z_0 \leq z \leq z_b)$$

where $W = U(z_0)V'(z_0) - U'(z_0)V(z_0)$.

The zero depth, source depth, receiver depth, and bottom depth are 0, z_0, z and z_b respectively. The zero depth may be set at the air-water interface or at some other convenient point. It represents the depth above which no sound is refracted or reflected to the receiver. The horizontal wave number is k, r is the horizontal distance between the source and receiver, J_0 is the Bessel function of the first kind of order zero, U is a solution of the z-separated part of the wave equation [i.e. $U'' = (k^2 - \omega^2/v^2(z))U$] that satisfies the boundary condition at z = 0, and v is a solution of the z-separated part of the wave equation [i.e. $V'' = (k^2 - \omega^2/v^2(z))V$] that satisfies the boundary condition at $z = z_b$. Formally our treatment will be restricted to $(z_0 \leq z \leq z_b)$, however, a similar development for $(0 \leq z \leq z_0)$ is easily derived.

It is easy to show that dW/dz is zero so that W is independent of depth. Also, we are free to specify the value of U and V at one depth. For convenience replace U and V by $\bar{U}$ and $\bar{V}$ where $\bar{U}(z_b) = \bar{V}(z_b) = 1$. It

follows then that in the limit $z_p \to z_b$ $W = W_{z_b} = [i \ell_b(1-R) - (1+R) \bar{U}'(z_b)]/(1+R)$. Therefore ψ can be expressed as

$$\psi = -2 \int_0^\infty \frac{(1+R)\, \bar{U}(z_0)\, \bar{V}(z)\, J_0(kr)\, kdk}{(i\ell_b - \bar{U}'_{z_b}) - R(i\ell_b + \bar{U}'_{z_b})} .$$

For the general sound speed profile it does not appear feasible to separate the direct sound paths from the bottom reflected paths. However, if the water has a constant sound speed then $\bar{U}(z) = \exp[i\ell(z_b - z)]$ and $\bar{V}(z) = [\exp - i\ell(z_b - z) + R \exp i\ell(z_b - z)]/(1+R)$. In this case it follows that

$$\psi = \underbrace{\int_0^\infty (i/\ell) e^{i\ell(z-z_0)} J_0(kr)\, kdk}_{\psi_D} + \underbrace{\int_0^\infty (i/\ell) R e^{i\ell(2z_b - z - z_0)} J_0(kr)\, kdk}_{\psi_R}$$

If the bottom reflected field ψ_R can be measured directly then we have

$$\psi_R = \int_0^\infty (i/\ell)\, R e^{i\ell(2z_b - z - z_0)} J_0(kr)\, kdk$$

and R can be determined experimentally by use of the Hankel Transform

$$R = \int_0^\infty \psi_R\, J_0(kr)\, rdr / [(i/\ell) \exp i\ell(2z_b - z - z_0)] .$$

This is not a practical procedure, however, because quadrature sampling would be required to determine the real and imaginary parts of ψ_R. That is Real $(\psi_R) = p_R \cos\phi$ and $\mathrm{Im}(\psi_R) = p_R \sin\phi$, where p_R is 1/2 the peak to peak pressure of the bottom reflected signal and ϕ is the phase. In any event when realistic profiles are considered it is not possible to separate the direct and bottom reflected paths at low frequencies.

APPENDIX B: Calculation of R for Many Solid Layers Using Knopoff's Method

The standard methods of solution (i.e. transfer matrices or matrix inversion) are not useable for the many solid layer model because of accuracy, computer storage, and computer run time problems. In this index we show how the fast and accurate methods developed in earth wave problems can be modified for calculation of R. In particular we will use the fast algorithm of Schwab (1970) which is based on Knopoff's formulation (Knopoff, 1964). The notation used is that of Haskell (1953).

Referring to Fig. 10 we choose the potential function for the up- and down-going compressional waves in the layer to be

$$\phi_n = \frac{1}{\omega} [i A_n \cos p_n + B_n \sin p_n] \exp[i(\omega t - kx)],$$

where $p_n = k r_{\alpha n} z_n$.

Also, we choose the potential function describing the up- and down-going shear waves to be

$$\Psi_n = \frac{1}{\omega} [C_n \sin q_n + i D_n \cos q_n] \exp[i(\omega t - kx)],$$

where $q_n = k r_{\beta n} z_n$.

The components of motion and stress in the n^{th} layer are therefore

$$c \dot{U}_n = A_n \cos p_n - i B_n \sin p_n + r_{\beta n} C_n \cos q_n - i r_{\beta n} D_n \sin q_n ,$$

$$c\dot{W}_n = -i\, r_\alpha A_n \sin p_n + r_\alpha B_n \cos p_n + i\, C_n \sin q_n - D_n \cos q_n \ ,$$

$$\sigma_n = \rho_n(\gamma_n - 1)\, A_n \cos p_n - i\, \rho_n(\gamma_n - 1)\, B_n \sin p_n$$

$$+ \rho_n \gamma_n r_{\beta n} C_n \cos q_n - i\, \rho_n \gamma_n r_{\beta n} D_n \sin q_n \ ,$$

$$\tau_n = i\, \rho_n \gamma_n r_{\alpha n} A_n \sin p_n - \rho_n \gamma_n r_{\alpha n} B_n \cos p_n$$

$$- i\, \rho_n(\gamma_n - 1)\, C_n \sin q_n + \rho_n(\gamma_n - 1)\, D_n \cos q_n \ .$$

In the above c is the horizontal phase velocity ($c = \omega/k$), $\dot{U}_n$ and $\dot{W}_n$ are the horizontal and vertical components of particle velocity, σ_n is the normal (vertical) stress, and τ_n is the tangential (horizontal) stress.

By separating ϕ_0 into an incident and reflected wave it is easy to show that the plane wave reflection coefficient R is given by

$$R = (A_0 - B_0)/A_0 + B_0) \ .$$

For convenience we set the value of $A_0 \equiv 1$. The three interface conditions at the water/sediment layer 1 interface can be written as

$$r_{\alpha 0} B_0 = r_{\alpha 1} B_1 - D_1 \qquad \text{(cont. of } \dot{W}\text{)}$$

$$-\rho_0 = \rho_1(\gamma_1 - 1)A_1 + \rho_1 \gamma_1 r_{\beta 1} C_1 \qquad \text{(cont. of } \sigma\text{)}$$

$$0 = -\rho_1 \gamma_1 r_{\alpha 1} B_1 + \rho_1(\gamma_1 - 1)\, D_1 \qquad \text{(cont. of } \tau\text{)}$$

Divide the last 2 above equations by ρ_1 and form the matrix of coefficients of B_0, A_1, B_1, C_1, D_1 (this is Knopoff's fast form).

B_0	A_1	B_1	C_1	D_1	
$r_{\alpha 0}$	0	$-r_{\alpha 1}$	0	1	$= 0$
0	$(\gamma_1 - 1)$	0	$\gamma_1\ r_{\beta 1}$	0	$= -\rho_0/\rho_1$
0	0	$-\gamma_1\ r_{\alpha 1}$	0	$(\gamma_1 - 1)$	$= 0$

Now modify the basis vectors so that the interface conditions can be within in the following matrix form

$$\begin{bmatrix} 1 & 0 & -1 & 0 & +1 \\ 0 & (\gamma_1-1) & 0 & \gamma_1 & 0 \\ 0 & 0 & -\gamma_1 & 0 & (\gamma_1-1) \end{bmatrix} \times \begin{bmatrix} B_0\ r_{\alpha 0} \\ A_1 \\ B_1\ r_{\alpha 1} \\ C_1\ r_{\beta 1} \\ D_1 \\ A_2 \end{bmatrix} = \begin{bmatrix} 0 \\ -\rho_0/\rho_1 \\ 0 \\ 0 \\ 0 \\ 0 \end{bmatrix}$$

Now solve for B_0 using Cramer's Rule

$$B_0\ r_{\alpha 0} = \frac{\begin{vmatrix} 0 & 0 & -1 & 0 & +1 \\ -\rho_0/\rho_1 & & & & \\ 0 & & \Delta_R & & \\ 0 & & & & \end{vmatrix}}{\begin{vmatrix} 1 & 0 & -1 & 0 & -1 \\ 0 & & & & \\ 0 & & \Delta_R & & \\ 0 & & & & \end{vmatrix}}$$

The elements inside the dashed areas designated Δ_R are the elements of the Rayleigh determinant. Fast and accurate methods are finding $|\Delta_R|$ have been developed (as mentioned before) because the zeroes of $|\Delta_R|$ determine the phase velocity of earthquake waves. Finally we can write

$$\frac{B_0\, r_{\alpha 0}}{(\rho_0/\rho_1)} = \frac{\begin{vmatrix} 0 & -1 & 0 & 1 \\ 0 & -\gamma_1 & 0 & (\gamma_1 - 1) \end{vmatrix}}{\begin{vmatrix} \gamma_1 - 1 & 0 & \gamma_1 & 0 \\ 0 & -\gamma_1 & 0 & (\gamma_1 - 1) \end{vmatrix}} \cdot = \frac{|\Delta_S|}{|\Delta_R|}$$

In the above $|\Delta_R|$ is the Rayleigh determinant and $|\Delta_S|$ is the same except for the first row. The fast methods developed for calculation of $|\Delta_R|$ can be used to evaluate $|\Delta_S|$. It follows then that the plane wave reflection coefficient can be written as

$$R = (\rho_1\, r_{\alpha 0}\, |\Delta_R| - \rho_0\, |\Delta_S|)/(\rho_1\, r_{\alpha 0}\, |\Delta_R| + \rho_0\, |\Delta_S|) \quad .$$